Hindawi Publishing Corporation
Journal of Nanoparticles
Volume 2014, Article ID 734256, 7 pages
http://dx.doi.org/10.1155/2014/734256

*Research Article*

# Optical and Structural Properties of ZnO Nanoparticles Synthesized by $CO_2$ Microwave Plasma at Atmospheric Pressure

**Se Min Chun, Dae Hyun Choi, Jong Bae Park, and Yong Cheol Hong**

*Plasma Technology Research Center, National Fusion Research Institute, 814-2 Osikdo-dong, Gunsan, Jeollabuk-do 573-540, Republic of Korea*

Correspondence should be addressed to Yong Cheol Hong; ychong@nfri.re.kr

Received 26 February 2014; Accepted 21 April 2014; Published 23 June 2014

Academic Editor: Xiangwu Zhang



The results of carbon-doped zinc oxide nanoparticles synthesized by $CO_2$ microwave plasma at atmospheric pressure are presented. The 2.45-GHz microwave plasma torch and feeder for injecting Zn granules are used in the synthesis of zinc oxide nanoparticles. The Zn granules (13.5 g/min) were introduced into the microwave plasma by $CO_2$ (5 l/min) swirl gas. The microwave power delivered to the $CO_2$ microwave plasma was 1 kW. The synthesis of carbon-doped zinc oxide nanoparticles was carried out in accordance with $CO_2 + Zn \rightarrow$ carbon-doped ZnO + CO. The synthesized carbon-doped zinc oxide nanoparticles have a high purity hexagonal phase. The absorption edge of carbon-doped zinc oxide nanoparticles exhibited a red shift from a high-energy wavelength to lower in the UV-visible spectrum, due to band gap narrowing. A UV-NIR spectrometer, X-ray diffraction, emission scanning electron-microscopy, energy dispersive X-ray microanalysis, Fourier transform infrared spectroscopy, and a UV-Vis-NIR spectrophotometer were used for the characterization of the as-produced products.

## 1. Introduction

$CO_2$ has been verified as a significant factor in the increase of the greenhouse effect. The decomposition and extinction of $CO_2$ are very important to environmental factors. Recently, $CO_2$ capture and storage (CCS) [1, 2], $CO_2$ capture and utilization (CCU) [3], and $CO_2$ reforming of $CH_4$ [4] are being used as technology for recycling $CO_2$. CCU is among the more promising of these technologies being deployed. In order to utilize the oxygen in $CO_2$ as an oxidant, the synthesis method of carbon-doped zinc oxide nanoparticles (C-doped ZnO-NPs) using a $CO_2$ microwave plasma torch has been designed. The developed $CO_2$ microwave plasma torch operated at atmospheric pressure seems to have demonstrated high potential for the synthesis of C-doped ZnO. The UV near-band edge emission of pure ZnO catalyst is detected in approximately 380 nm (~3.2 eV). Therefore, a band gap of Pure ZnO does not allow the capture of most of the solar light energy [5]. Only a small portion (UV energy) of the solar spectrum is absorbed. Consequently, a major issue of ZnO catalyst production is the need to increase the efficiency of photo-activity by band gap narrowing. The band gap narrowing of photo-catalyst is obtained by the inclusion of transition metals (V, Cr, Mn, and Fe) or main group atoms (N, C, S, and F). As a typical example, impurities such as transition metals, nitrogen, sulphur, and carbon can be doped in oxygen vacancy or the lattice of a ZnO catalyst using one of several synthesis ways. Various transition metal cations have been introduced to extend the optical absorption of ZnO-NPs to the visible light region. We designed the synthesis system of C-doped ZnO-NPs using $CO_2$ microwave plasma torch. The synthesis of C-doped ZnO-NPs is carried out according to $CO_2 + Zn \rightarrow$ C-doped ZnO + CO. The Zn granules are introduced into the $CO_2$ microwave plasma as a precursor. The ZnO-NPs are synthesized immediately by the chemical species with high reactivity and the high-temperature of the $CO_2$ microwave plasma. In this paper, a method for the production of C-doped ZnO-NPs via synthesis by the use of a $CO_2$ microwave plasma torch operated at atmospheric pressure is presented.

## 2. Experimental Methods

The process of the preparation of C-doped ZnO-NPs is as illustrated in Figure 1. The synthesis system has been presented elsewhere [6–8] and has been employed to synthesize carbon nanotube, iron oxide, and titanium nitride. As shown in Figure 1, the main parts of the experimental setup used in this investigation were a 2.45-GHz microwave power system, a gas and Zn granules supplying system, and a $CO_2$ microwave plasma torch. The reactive energy from a microwave generator is supplied to the flowing gas for the generation of $CO_2$ microwave plasma at atmospheric pressure. An efficient microwave power transfer from a magnetron can be achieved via an isolator, a directional coupler, a 3-stub tuner, and a tapered waveguide. The center axis of the quartz tube (outer diameter of 30 mm, thickness of 2 mm, and length of 90 mm) is located a one-quarter wavelength from the short end of the waveguide wall, which is connected to a stainless steel pipe (length of 700 mm). The $CO_2$ microwave plasma generates in a quartz tube inserted perpendicularly to the wide waveguide where the induced electric field peak is at its highest. The maximization of the electric field induced by the microwave radiation in the quartz tube can be controlled by the 3-stub tuner. Additionally, the reflected power is minimized by adjusting the 3-stub tuner and is less than 1% of the forward power.

All the gas flows are controlled by mass flow controllers (MFCs). $CO_2$ as swirl gas (15 L/min) and 1 kW of microwave power were used for the generation of pure $CO_2$ microwave plasma. The swirl gas was injected into the $CO_2$ microwave plasma torch via four small holes in tangential direction. The main purposes of the swirl gas are the maintenance and stabilization of $CO_2$ microwave plasma in the inner surface of the quartz tube. Without swirl, the plasmas damage the inner wall of the quartz tube.

The Zn granules (99.8%, Aldrich) of a mean size of 1.2 mm are introduced via the feeder. The feeder was positioned roughly ~20 mm from the upper wall of the tapered waveguide. When the Zn granules make contact with the $CO_2$ microwave plasma flame, the Zn species is vaporized by high-temperature flame and then explosively reacts with atomic oxygen and oxygen-related species produced in the $CO_2$ microwave plasma. Furthermore, the $CO_2$ microwave plasma flame endows the doping of carbon species into ZnO particles simultaneously. The ZnO-NPs generated by the $CO_2$ microwave plasma torch were deposited in the inner wall of a stainless steel pipe.

Figure 2(a) shows a typical $CO_2$ plasma flame generated at the applied power of 1 kW. The $CO_2$ plasma flame is divided into two distinctive regions: a bright, whitish region and bluish region. The bright, whitish region is a typical high-temperature region, which corresponds to the region of the dissociation of $CO_2$ into various chemical species, as shown in the plasma emission spectra of Figure 2(b). The other is the recombination zone for carbon monoxides to burn in the oxygen species. Figure 2(b) depicts the optical emission spectra of a typical $CO_2$ plasma flame corresponding to Figure 2(a). The HR4000CG-UV-NIR spectrometer in this test was employed for the measurement of the relative intensities of chemical species in the $CO_2$ plasma, along with the different axial positions of the plasma column. The positions of emission analysis have measured at 15 mm intervals from upper tapered waveguide wall. The $CO_2$ microwave plasma emissions are predominant with the carbon molecules ($C_2$) in 400–600 nm, atomic oxygen in 777, 844, and 925 nm and atomic carbon, carbon radicals, and $CO_2$ in the UV region. As the distance increases from the bright plasma region, a broad molecule spectrum mainly occurs, corresponding to molecules $CO_2$ and CO. Furthermore, the microwave plasma at atmospheric pressure is one of the plasma techniques providing an electron temperature of 4000–10000 K and a heavy particle temperature of 2000–6000 K [9–11]. Therefore, oxidation reactions of the Zn species and oxygen radicals ($O^*$) occurred more actively at the bright region of $CO_2$ microwave plasma. We expected that carbon-related chemical species would be incorporated into ZnO crystals.

In order to investigate the characteristics of the synthesized ZnO-NPs, they were taken at different positions in the stainless steel pipe. As shown in Figure 2(c), the synthesized ZnO-NPs were collected from the inner wall of the stainless steel pipe and divided into three regions. This was because samples A–C correlate with different $CO_2$ microwave plasma flame regions.

For characteristic analysis of the as-synthesized sample, a Shimadzu 3600 type UV-Vis spectrophotometer and a Bruker D8 advance 40 kW X-ray diffractometer with Cu K$\alpha$ radiation at a scan rate of $0.5^\circ 2\theta s^{-1}$ were employed. In order to observe the surface morphology and the elements of the samples, a ZEISS microscope field emission scanning electron-microscopy (FE-SEM) on SIGMA operating at an accelerating voltage of 10 kV and Thermo Scientific Energy Dispersive X-ray microanalysis (EDX) were employed. All the samples were prepared by sonicating as-produced powder in alcohol for 30 minutes. To obtain an FE-SEM image, a drop of the thus formed suspension was placed on a TEM grid covered with a thin Silicon film and dried in air.

## 3. Results and Discussion

This synthesis method enhanced by the $CO_2$ microwave plasma torch was employed in the production of C-doped ZnO-NPs. As previously mentioned, the microwave plasma provides radical and reactive species at high temperatures. Therefore, the ZnO-NPs can be formed in a very short time at high temperature and deposited on the inner wall of the stainless steel pipe. The diagnostics of the C-doped ZnO-NPs showed that the photo catalyst efficiency of synthesized samples improved via an investigation of optical and morphological properties.

The X-ray diffraction (XRD) was employed to compare the lattice phase of as-produced ZnO-NPs at different regions of the $CO_2$ microwave plasma flame. Figures 3(a)–3(c) show the XRD patterns of three ZnO samples synthesized at different regions corresponding to samples A–C in Figure 2(c), respectively. All samples have similar XRD patterns. All the reflections can be indexed to a pure hexagonal phase of ZnO

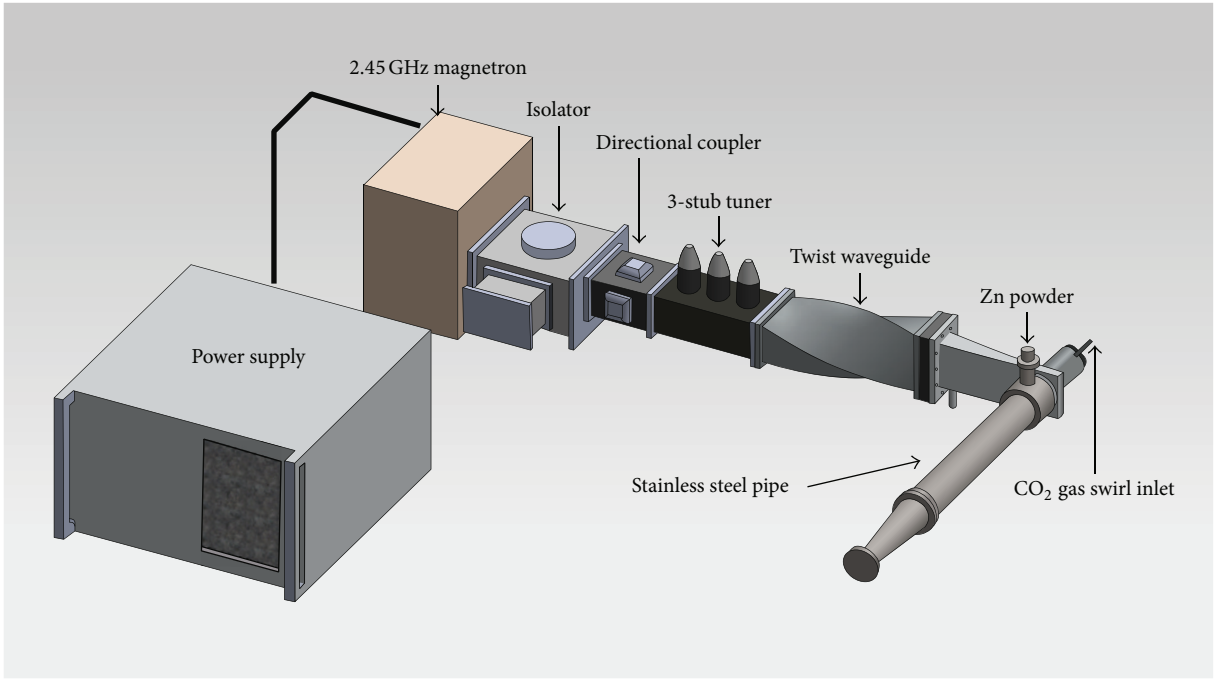


Figure 1: Schematic diagram of the experimental setup with the $CO_2$ microwave plasma torch.

Table 1: EDX analysis of the synthesized ZnO-NPs.

| Element line | Atom (%) | | | |
|---|---|---|---|---|
| | A | B | C | D |
| C | 3.00 | 2.76 | 9.64 | 2.37 |
| O | 41.25 | 40.79 | 42.46 | 48.02 |
| Zn | 55.75 | 56.46 | 47.89 | 49.61 |
| Total | **100** | **100** | **100** | **100** |

(space group: $P6_3mc$ (186)) with lattice constants $a = 3.248$ Å and $c = 5.206$ Å, which are in agreement previously with the reported data (JCPDS file No. 36-1451) [12]. As shown in Figure 3, no characteristics peaks were observed, revealing the near perfect conversion of Zn granules to ZnO-NPs, even if only a small phase of Zn was measured. In addition, the result from XRD revealed that the ZnO-NPs produced are single-phase hexagonal ZnO. The synthesized ZnO-NPs (sample A) in the bright region of $CO_2$ plasma indicate higher purity of the ZnO hexagonal phase because of strong plasma intensities. The crystallite sizes ($\tau$) were calculated using the Scherrer equation [13], $\tau = K\lambda/\beta\cos\theta$, where $\beta$ is the breadth of the observed diffraction line at its half-intensity maximum, $K$ the so-called shape factor, which usually takes on a value of about 0.9, and $\lambda$ the wavelength of the X-ray source used in XRD. Therefore, crystal sizes calculated from XRD line-broadening using the Scherrer formula with a shape factor of 0.9 are (a) 90, (b) 73, and (c) 60 nm, respectively. As the distance of collected samples increases, particle sizes become smaller.

Table 1 illustrates the EDX analysis of all elements in the synthesized ZnO-NPs. The analysis data listed in Table 1 shows the entire amounts of all elements. According to the EDX analysis of C-doped ZnO-NPs, all samples contain Zn, O, and C species. Compared with sample D, samples A–C have to contain more carbon species. All of the synthesized samples show content of carbon higher than commercial sample D. This is because the carbon of samples A–C is doped by $CO_2$ microwave plasma, whereas sample D only includes a weak C species originating from carbon contamination of the air. Consequentially, the C species of C-doped ZnO-NPs are filled by singly oxygen vacancies. Sample C among all samples, in particular, contains a large amount of carbon. The synthesized ZnO-NPs deposition commenced immediately after plasma ignition. However, not all ZnO-NPs were deposited on the front of the stainless steel pipe. The synthesized ZnO-NPs in major parts were blown off the stainless steel pipe by the high plasma flow. For this reason, ZnO-NPs containing a large amount of carbon can be deposited on the end of a stainless steel pipe.

Figures 4(a)–4(c) show the FE-SEM images of the as-produced ZnO-NPs corresponding to samples A–C in Figure 2(c), respectively. The FE-SEM image of ZnO-NPs in Figure 4(a) shows that ZnO-NPs are agglomerated by the high temperature of the $CO_2$ microwave plasma. On the other hand, as shown in Figure 3(c), the structure of ZnO-NPs can consist of rod, tripod, and irregular shapes. The inset of Figure 3(c) shows a close-up image of synthesized ZnO-NPs of a tripod shape with an approximate average length of around ~100 nm. The changed shape of the particles depending on the synthesized region is regarded as an effect of the microwave plasma temperature and carbon content in ZnO-NPs.

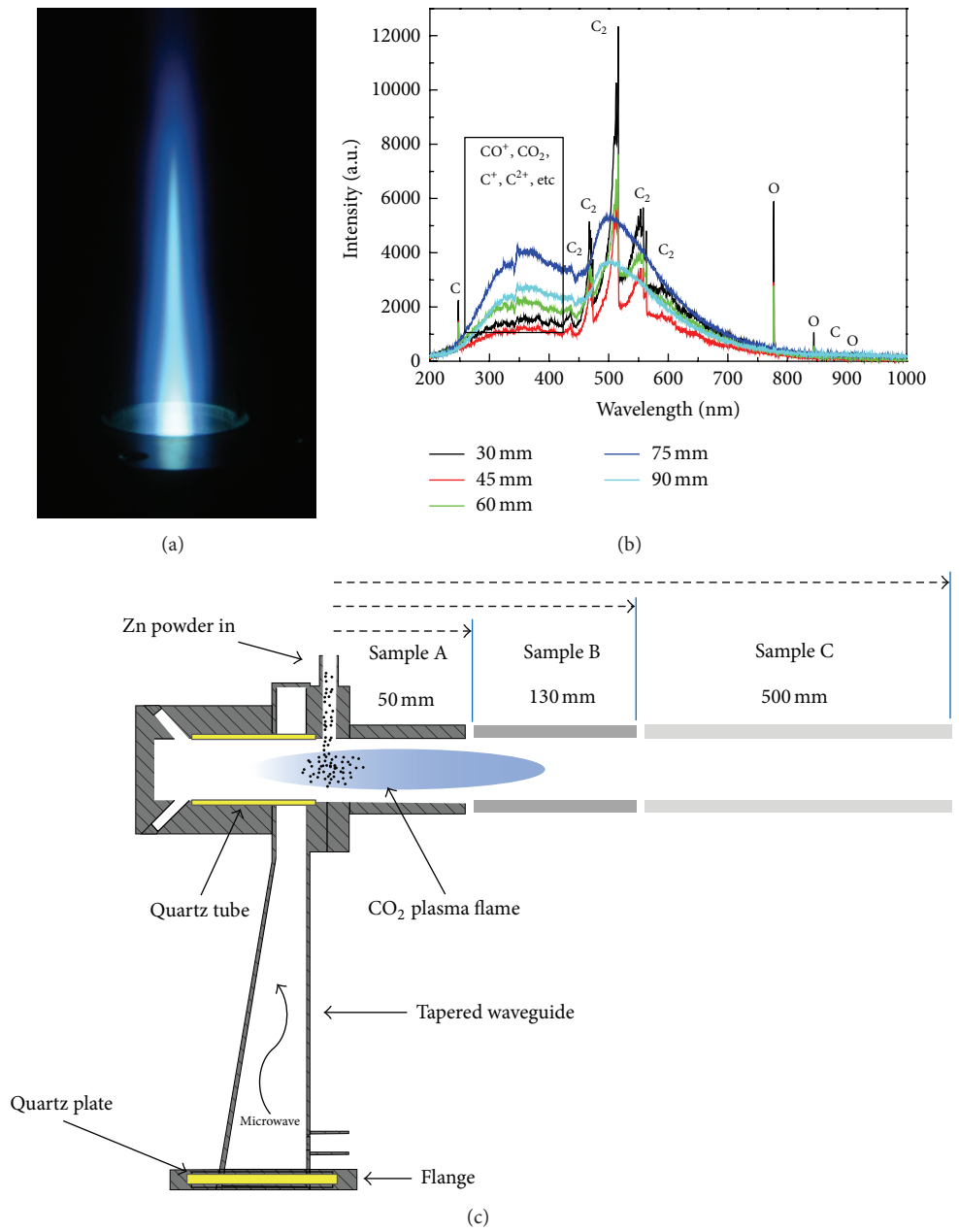


FIGURE 2: (a) The $CO_2$ microwave plasma flames produced from the 2.45 GHz plasma torch are divided into two distinctive regions, composed of bright, whitish and blue regions. (b) Emission spectra according to the Z-axis direction of the $CO_2$ microwave plasma flame. (c) Samples A–C decided according to the region type in $CO_2$ plasma flames.

Figure 5 shows the Fourier transform infrared spectroscopy (FT-IR) spectrum of the synthesized ZnO by $CO_2$ microwave plasma. Approximately, the band related to the ZnO bonds of samples A–C was observed. The CH stretching band at the 3000–2800 $cm^{-1}$ region was detected, illustrating the bonding between carbon in ZnO and moisture in the atmosphere. Therefore, we believe that the as-produced sample was doped with carbon-species. Furthermore, the absorbance band of HOH at 1625 $cm^{-1}$ is indicated by the absorption of $H_2O$ in the air. Both OH (below 3500 $cm^{-1}$) and HOH modes are strongly perturbed relative to the gas-phase spectrum of $H_2O$ [14].

For an accurate measurement concerning the oxygen vacancy in C-doped ZnO-NPs, we compared the UV-visible spectra with samples A–C. Figure 6 shows the UV-visible spectra of the synthesized ZnO-NPs corresponding to samples A–C in Figure 2(c), which indicates a closed-up spectrum of visible emissions between 350 and 700. The UV near-band edge emission is due to an exciton-related transition [15, 16]. Figure 6 shows that the synthesized samples noticeably absorb the light at 420, 440, and 480 nm, respectively,

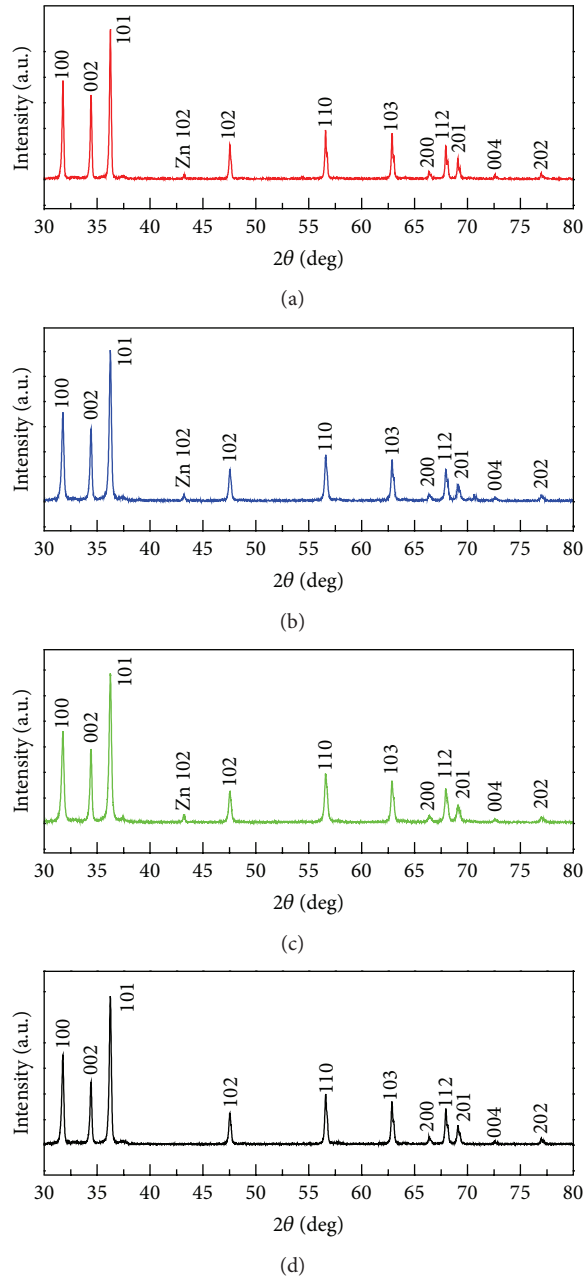


FIGURE 3: (a)–(c) are the XRD patterns corresponding to samples A–C of Figure 2(c), respectively. (d) is the XRD pattern of a commercial ZnO.

whereas the commercial sample (d) does not, which adheres to the theoretical results. In other words, all of the synthesized ZnO-NPs showed a significant red shift in the absorption edge to lower energy due to band gap narrowing. On the one hand, the amount of carbon increases and the effective influence of red shift was predicted. Sample (c) contained a large amount of carbon, illustrating more than a red shift in Figure 6.

## 4. Conclusions

The novel C-doped ZnO-NPs were synthesized by a $CO_2$ microwave plasma torch at atmospheric-pressure. Results from this experiment demonstrate that the $CO_2$ microwave plasma torch is a good method to use for the synthesis of C-doped ZnO-NPS. The $CO_2$ gas was used as a carbon source and oxidant. The C-doped ZnO-NPs with sizes around ~100 nm were rapidly synthesized by the oxidation reaction of Zn vapor and radicals produced in the high temperature flame of the $CO_2$ microwave plasma. Only the hexagonal ZnO phase was detected by XRD pattern. The C-doped ZnO-NPs were of a nanorod-like structure, such as a rod or tripod, and the average length of tripod was approximately ~100 nm. The average particle size was approximately the same as the calculated value according to the Scherrer formula. It was identified that the synthesized ZnO-NPs include carbon

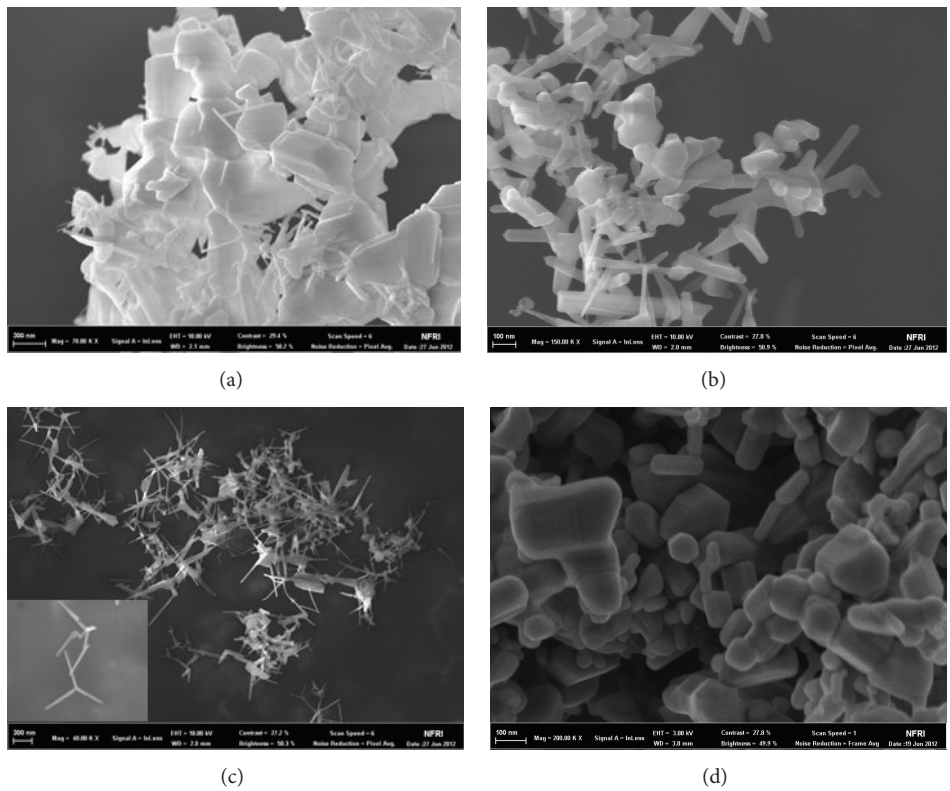


Figure 4: (a)–(c) are the FE-SEM images corresponding to the sample A–C in Figure 2(c), respectively. (d) is the FE-SEM image of a commercial ZnO.

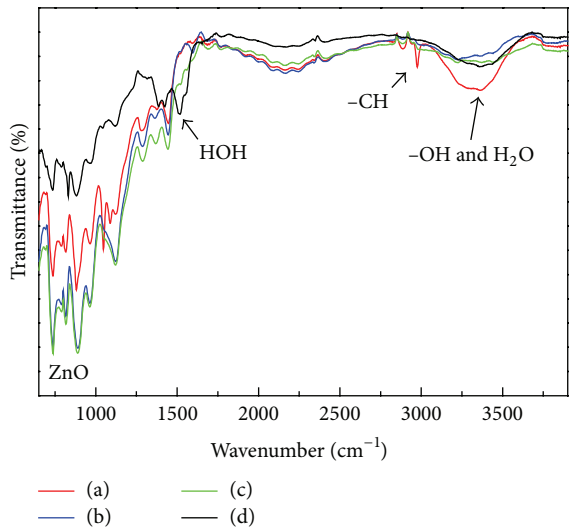


Figure 5: (a)–(c) are the FT-IR spectra corresponding to samples A–C in Figure 2(c), respectively. (d) is the FT-IR spectrum of a commercial ZnO.

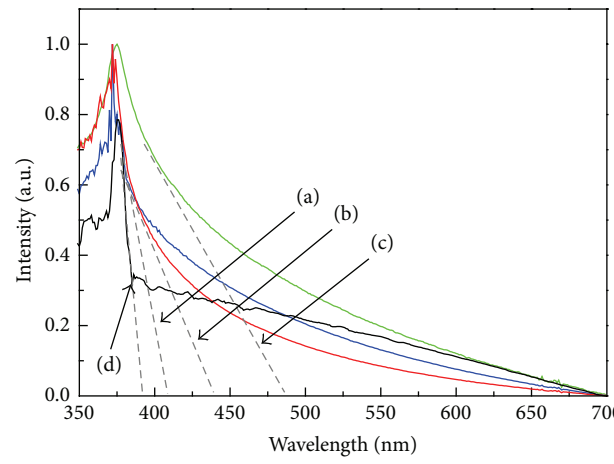


Figure 6: UV-visible spectrum of ZnO-NPs corresponding to samples (a)–(c). (d) is the UV-visible spectrum of a commercial ZnO.

species. Carbon species are incorporated into the O site of ZnO in the process of synthesis. For comparison, commercial ZnO was also prepared. It was found that C-doped ZnO exhibited a significant red shift to the visible region. We expect to the improved photo-catalytic activity of C-doped ZnO better than commercial ZnO on the visible light region. The study of the photo-reaction of C-doped ZnO will be placed on the future research.

## Conflict of Interests

The authors declare that there is no conflict of interests.

## Acknowledgments

This work was supported by an R&D Program through the National Fusion Research Institute of Korea (NFRI) funded by the government and also was supported by the 2013 R&D Convergence Program funded by Korea Research Council of Fundamental Science & Technology (R&D Convergence-13-6-NFRI).

## References

[1] H. H. Lamb, *Climate: Present, Past and Future: Fundamentals and Climate Now*, vol. 1, Methuen, London, UK, 1972.

[2] P. Riemer, "Greenhouse gas mitigation technologies, an overview of the $CO_2$ capture, storage and future activities of the IEA Greenhouse gas R&D programme," *Energy Conversion and Management*, vol. 37, no. 6–8, pp. 665–670, 1996.

[3] K. M. K. Yu, I. Curcic, J. Gabriel, and S. C. E. Tsang, "Recent advances in $CO_2$ capture and utilization," *ChemSusChem*, vol. 1, no. 11, pp. 893–899, 2008.

[4] M. C. J. Bradford and M. A. Vannice, "$CO_2$ reforming of $CH_4$," *Catalysis Reviews—Science and Engineering*, vol. 41, no. 1, pp. 1–42, 1999.

[5] C. Kormann, D. W. Bahnemann, and M. R. Hoffmann, "Preparation and characterization of quatum-size titanium dioxide," *Journal of Physical Chemistry*, vol. 92, no. 18, pp. 5196–5201, 1988.

[6] Y. C. Hong, T. Lho, B. J. Lee, H. S. Uhm, O. Kwon, and S. H. Lee, "Synthesis of titanium dioxide in $O_2/Ar/SO_2/TiCl_4$ microwave torch plasma and its band gap narrowing," *Current Applied Physics*, vol. 11, no. 3, pp. 517–520, 2011.

[7] Y. C. Hong, T. H. Lho, D. H. Shin, and H. S. Uhm, "Removal of fluorinated compound gases by an enhanced methane microwave plasma burner," *Japanese Journal of Applied Physics*, vol. 49, no. 1R, Article ID 017101, 2010.

[8] H. S. Uhm, Y. C. Hong, D. H. Shin, and B. J. Lee, "Plasma-enhanced gasification of low-grade coals for compact power plants," *Physics of Plasmas*, vol. 18, no. 10, Article ID 104505, 2011.

[9] K. M. Green, M. Cristina Borrás, P. P. Woskov, G. J. Flores III, K. Hadidi, and P. Thomas, "Electronic excitation temperature profiles in an air microwave plasma torch," *IEEE Transactions on Plasma Science*, vol. 29, no. 2, pp. 399–406, 2001.

[10] H. S. Uhm, Y. C. Hong, and D. H. Shin, "A microwave plasma torch and its applications," *Plasma Sources Science and Technology*, vol. 15, no. 2, pp. S26–S34, 2006.

[11] M. Jasiński, M. Dors, and J. Mizeraczyk, "Production of hydrogen via methane reforming using atmospheric pressure microwave plasma source with $CO_2$ swirl," *International Journal of Engineering Science and Technology*, vol. 2, no. 2, pp. 134–139, 2008.

[12] X. L. Hu, Y. J. Zhu, and S. W. Wang, "Sonochemical and microwave-assisted synthesis of linked single-crystalline ZnO rods," *Materials Chemistry and Physics*, vol. 88, no. 2-3, pp. 421–426, 2004.

[13] R. Jenkins and S. L. Snyder, "Introduction to X-ray powder diffractometry," J. K. Winefordner, Ed., p. 89, John Wiley & Sons, New York, NY, USA, 1996.

[14] K. S. Lee, S. H. Nam, H. O. Seo, Y. D. Kim, and J. H. Boo, "Surface property change of C doped $TiO_2$ nano-pillars by $O_2$ plasma treatment," *Journal of Nanoscience and Nanotechnology*, vol. 11, no. 12, pp. 10599–10603, 2011.

[15] Y. R. Ryu, S. Zhu, J. D. Budai, H. R. Chandrasekhar, P. F. Miceli, and H. W. White, "Optical and structural properties of ZnO films deposited on GaAs by pulsed laser deposition," *Journal of Applied Physics*, vol. 88, no. 1, pp. 201–204, 2000.

[16] Y. Chen, S. K. Hong, H. J. Ko, M. Nakajima, T. Yao, and Y. Segawa, "Plasma-assisted molecular-beam epitaxy of ZnO epilayers on atomically flat $MgAl_2O_4(111)$ substrates," *Applied Physics Letters*, vol. 76, no. 2, pp. 245–247, 2000.